Wicking and flooding of liquids on vertical porous sheets

Seong Jin Kim, Jin Woo Choi, Myoung-Woon Moon, Kwang-Ryeol Lee, Young Soo Chang, Dae-Young Lee, and Ho-Young Kim

Wicking and flooding of liquids on vertical porous sheets

Seong Jin Kim,[1] Jin Woo Choi,[2] Myoung-Woon Moon,[1,a)] Kwang-Ryeol Lee,[1] Young Soo Chang,[3] Dae-Young Lee,[1] and Ho-Young Kim[2,b)]
[1]*Korea Institute of Science and Technology, Seoul 136-791, South Korea*
[2]*Department of Mechanical and Aerospace Engineering, Seoul National University, Seoul 151-744, South Korea*
[3]*School of Mechanical Systems Engineering, Kookmin University, Seoul 136-702, South Korea*

When one brings a wet paintbrush into contact with a vertical watercolor paper, the paint may wick into the porous sheet completely or run down to ruin the art. We study a simple model of this spreading dynamics of liquids on hydrophilic porous sheets under the effects of gravity, using a capillary as a liquid source and thin fabrics of non-woven polyethylene terephthalate. Upon finding the maximum flow rate, Q_w, that can be absorbed into the fabric, we show that the model can be used to obtain an estimate of the in-plane permeability of fabrics in a simpler manner than the conventional schemes. The shape of a wetting area that grows when the flow rate exceeds Q_w to lead to rivulet formation is also theoretically given. The nose shape of the wetting front is shown to be time-invariant, while its profile depends on the properties of the liquid and the fabric. This study can be applied to understand and improve the liquid absorption behavior of hygiene items, heating, ventilation, and air-conditioning equipments, and fuel cell membranes in addition to elucidating the mundane painting activity. © 2015 AIP Publishing LLC.
[http://dx.doi.org/10.1063/1.4914384]

I. INTRODUCTION

The spreading of liquids on solid surfaces is an essential process in a variety of practical applications including painting, printing, composite manufacturing,[1] paper-based microfluidics,[2] absorption in hygiene items,[3] and HVAC (heating, ventilation, and air-conditioning) technology.[4,5] Complete wetting of solids helps, for example, to prevent void formation in composite manufacturing, to accelerate the liquid transport in microfluidic systems, and to enhance the heat and mass transfer rate between liquid films and gas in some HVAC equipments including liquid desiccant air dehumidifiers.[4] In fuel cell systems employing proton exchange membranes, the water absorption characteristics of the porous gas diffusion layer play a critical role in preventing water flooding and keeping appropriate hydration level of the membrane.[6]

Our interest lies in the dynamics of liquid fed from a narrow source like a capillary on a *vertical* surface, a situation much more complex than when liquid is fed on a horizontal surface because of the gravitational effects. Besides the practical applications where the vertically standing walls are to absorb liquid, this process determines what happens when one touches a wet paintbrush on a vertical paper. The outcome is drastically different depending on how well the liquid can be absorbed in the sheet—either a dot forms or watercolor will run down to ruin the art. Also, the spreading dynamics of liquids on a vertical surface play an important role in water ingestion of some animals living in arid environments, such as desert horned lizards, *Phrynosoma platyrhinos* of North America,[7] and desert lizards, *Moloch horridus* of Australia.[8] They need to retain as much water as possible on their rough body surface notwithstanding gravity.

---
a)Electronic mail: mwmoon@kist.re.kr
b)Electronic mail: hyk@snu.ac.kr

Here, we aim to establish a relationship between the liquid feeding rate and its spreading behavior on a vertical porous sheet, which depends on the flow rate and physical properties of the liquid and pore structures of the wettable solid. We first model and experimentally corroborate the wicking dynamics of liquid into a porous medium. This enables us to model the maximum flow rate that the porous body can absorb, which can lead to a novel scheme to obtain an estimate of an important property of porous media, permeability. Then, the hydrodynamics associated with flooding, that occurs when the flow rate exceeds the threshold value, is considered to predict the shape of the wet area elongating with time.

II. EXPERIMENTAL

We use a syringe pump (LSP04-1A, Baoding Longer Precision Pump) to feed different liquids, i.e., deionized water, ethylene glycol, and silicone oil, whose properties are listed in Table I, through a capillary of 0.41 mm in inner diameter onto a vertically situated sheet. Figure 1(a) depicts the schematic of the experimental setup. As vertical sheets, we use thin fabrics of non-woven PET (polyethylene terephthalate), whose structural properties are listed in Table II. The fabric is hydrophilized by air-plasma treatment in the plasma chamber (Cute, Femto Science). The equilibrium contact angles, θ_e, of a PET sheet with water, ethylene glycol, and silicone oil are measured by taking the angles between the tangents of the droplets of 5 μl volume and horizontal solid surface at the three-phase contact line. The values are 18°(water), 7°(ethylene glycol), and 6°(silicone oil) with the typical standard deviation of 3°. Figures 1(b)–1(d) show the microstructures of the PET fabrics. The average flow rate from the capillary varies from 0.03 to 49 cc/min. To observe the spreading behavior of liquids on smooth, in addition to rough, surfaces, we use a hydrophilized PET sheet.

III. WICKING VERSUS FLOODING

We start with a drop of the radius $a = 0.62$ mm, the air-liquid surface tension σ, and the density ρ placed on a vertical solid surface. The gravitational effect is negligible compared to the surface tension when $a < l_c = [\sigma/(\rho g)]^{1/2}$, where l_c is the capillary length. The spreading of a small drop on the vertical hydrophilic plane is hardly different from that on the horizontal hydrophilic plane as shown in Fig. 2, where we use deionized water drops and a PET sheet. We now turn to a continuous stream of liquid that is fed by a syringe pump onto a smooth vertically situated PET surface as shown in Fig. 3(a). A competition takes place between the gravitational force to pull the liquid downward and the capillary force to uniformly spread the liquid. Once the liquid volume exceeds a critical value that can be held up by the capillary forces, the liquid bulk forms and drains downward. Once the downward wet path is formed, liquid supplied afterwards keeps following the path.

Unlike the smooth surfaces which are able to hold only a minuscule volume of liquid against gravity, porous hydrophilic substrates can absorb significant amount of liquid without flooding. Figure 3(b) shows that a very wide circular blot can be formed when water is supplied on a hydrophilized non-woven PET fabric. The drastic difference between Figs. 3(a) and 3(b) results from the following two facts. First, the fabric absorbs the liquid into the spacing between the fibers, thereby allowing the liquid to occupy greater volume before drainage. Second, the capillary forces associated with imbition into hydrophilic porous media are much stronger than the uncompensated Young force[9] that is responsible for the spreading of liquids on smooth surfaces. Even on the

TABLE I. Physical properties of the liquids used in the experiments.

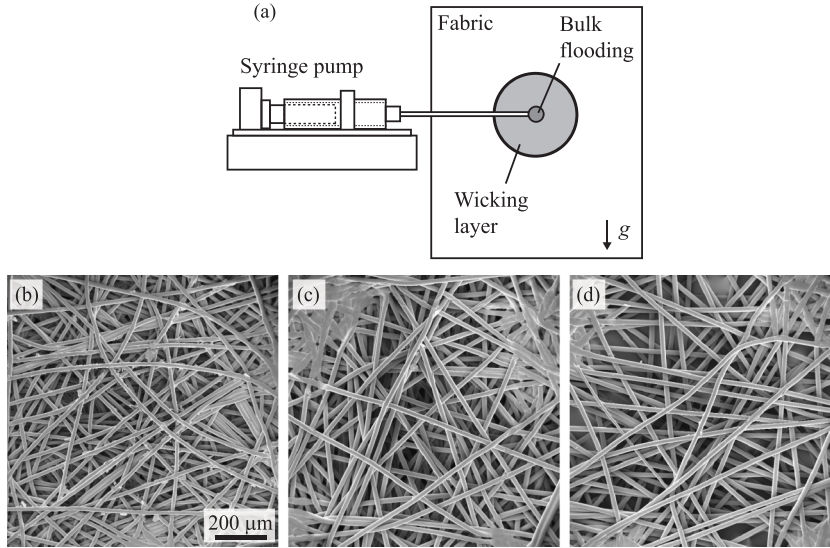|	Surface tension (N/m)	Viscosity (kg/m s)	Density (kg/m³)
Water	0.072	0.001	998
Ethylene glycol	0.047	0.016	1113
Silicone oil	0.022	0.088	979

FIG. 1. (a) Schematic of the experimental setup. SEM (scanning electron microscopy) images of non-woven PET fabrics I (b), II (c), and III (d).

porous substrate, however, the flooding occurs as shown in Fig. 3(c) when the flow rate exceeds a certain threshold.

To understand the criterion that determines whether the liquid would completely wick into pores as in Fig. 3(b) or flood as in Fig. 3(c), we consider the dynamics of wicking into hydrophilic porous media from an infinite point source. For a thin sheet which is rapidly wet throughout the thickness before any significant radial expansion of a blot occurs, the flow can be effectively assumed as planar. Then, the radius of the blot as shown in Fig. 3(b), R_w, follows the Darcy law:

$$\dot{R}_w = \frac{Q_w}{\phi A_c} \simeq \frac{\kappa}{\phi \mu} \frac{\Delta P}{R_w}, \tag{1}$$

where the dot denotes the time derivative, Q_w is the wicking flow rate, A_c is the area of the wet front perpendicular to the fabric plane of thickness c ($= 2\pi c R_w$), and μ is the dynamic viscosity of liquid. The in-plane permeability of the porous medium, κ, is the structural property depending on the porosity ϕ, pore size r, and the tortuosity of the fibers in case of fabrics.[10–12] Despite many attempts to give κ as a function of a single variable ϕ,[11–15] it is usually available only through experimental measurements. Although the pressure distribution can be given by solving the Laplace equation, we here use the average pressure gradient $\Delta P / R_w$, or the pressure drop over R_w, for mathematical simplicity. The pressure drop arising at the liquid-gas interface within porous media can be given in the form of $\Delta P = 2\sigma \cos \theta_e / r$ based on the assumption of the fabric structure as the regular array of cylindrical conduits with the equivalent hydraulic radius r.[10] Here, r can be estimated by use of two measurable parameters, ϕ and the fiber radius r_f, as $r = r_f \phi / (1 - \phi)$ based on the foregoing geometric assumption.[10] Assuming very small θ_e due to the hydrophilic plasma treatment, ΔP can be estimated as $\Delta P \approx 2\sigma (1 - \phi) / (r_f \phi)$.

TABLE II. Structural properties of the non-woven PET fabrics used in the experiments.

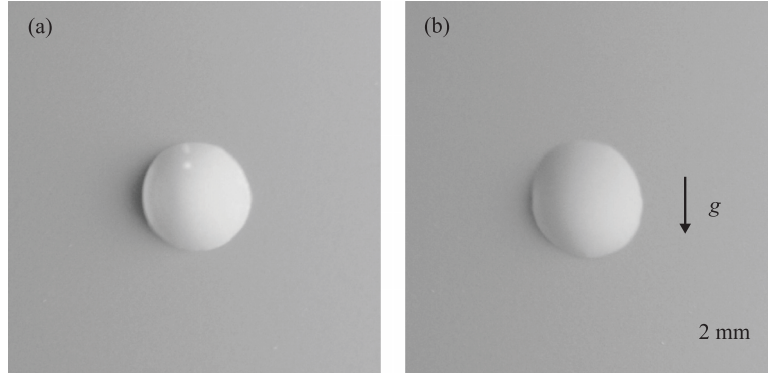|	Thickness (μm)	Porosity	Fiber radius (μm)
Fabric I	220	0.60	8.0
Fabric II	260	0.66	9.8
Fabric III	190	0.64	9.7

FIG. 2. Water drops on (a) the horizontal and (b) the vertical smooth hydrophilic PET sheets.

The relative importance of the gravitational force to the capillary force is measured by the Bond number defined as $\text{Bo} = \rho g b/(\sigma/r) = br/l_c^2$, where b is the lengthscale over which hydrostatic pressure develops – $b \sim r$ for complete wicking,[16] and $b \sim l$ for flooding with l corresponding to the length of the bulk in the direction of gravity. We find that $\text{Bo} \ll 1$ as long as $b \ll 0.5$, 0.3, and 0.1 m for water, ethylene glycol, and silicone oil, respectively, implying that the gravitational effect is negligible compared to capillarity in most of the current experimental conditions. On the other hand, when fabrics consisting of relatively big pores of millimeter-scales are used, hydrostatic effects become no longer negligible when b grows only to millimetric scales. Also, weak hydrophilicity increases the value of θ_e, leading to more pronounced effects of gravity. Such gravity-dominant liquid flows through porous media were treated previously.[17,18]

Integrating Eq. (1) gives the blot radius as a function of time t as

$$R_w \simeq 2\left[\frac{\kappa(1-\phi)}{r_f\phi^2} \frac{\sigma}{\mu}t \right]^{1/2}. \tag{2}$$

The wetting front propagates diffusively following Washburn's rule[19] with the prefactor of t besides σ/μ dependent on the fabric structure and permeability. We then get the flow rate of wicking, Q_w,

$$Q_w \simeq 4\pi \frac{c\kappa(1-\phi)}{r_f\phi} \frac{\sigma}{\mu}. \tag{3}$$

This formulation gives the flow rate from a point source that imposes no resistance to the wicking. For a large tube filled with liquid, the liquid would be sucked into the porous sheet at a rate given by Eq. (3), but the flow rate from the thin tube as used in this experiment is controlled by the syringe pump rather than the capillary force of the fabric. Typical of the circular spreading governed by the diffusive dynamics, the flow rate is constant throughout time.[20] Our analysis elucidates the functional dependency of Q_w on the fabric properties, $c\kappa(1-\phi)/(r_f\phi)$, and the liquid property, σ/μ. It is possible to regard Q_w as the maximum flow rate from a point source that can be absorbed
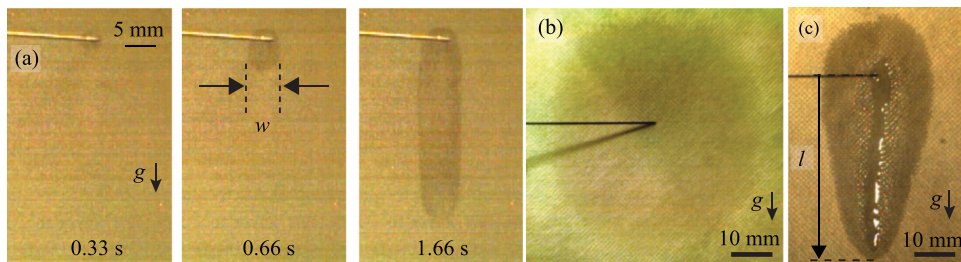

FIG. 3. Images of water blots supplied through a capillary on vertical substrates. (a) Smooth hydrophilic PET surface with the flow rate of 1 cc/min. Times are measured since the liquid starts to be fed. (b) Hydrophilized non-woven PET fabric I with the flow rate of 1.8 cc/min. (c) The identical non-woven PET fabric with the flow rate of 49 cc/min.
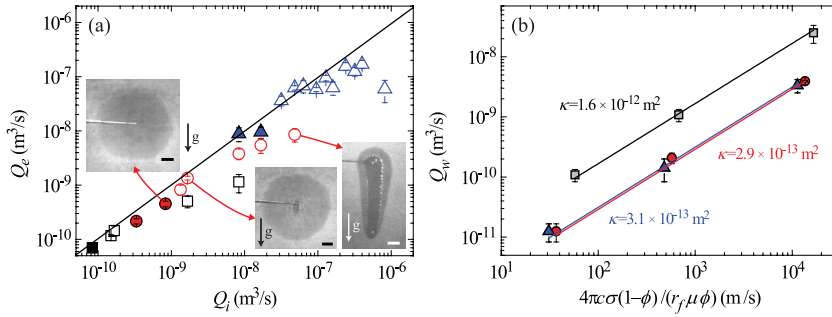
FIG. 4. (a) Flow rate calculated based on the wet area expansion, Q_e, versus the actual liquid supply rate, Q_i on PET fabric I. Filled symbols indicate the spreading without leaking a bulk and open ones with a leak. Black square, red circle, and blue triangle show the experiments using silicone oil, ethylene glycol, and water, respectively. Scale bars in the inserted pictures indicate 5 mm. (b) The threshold flow rate Q_w for different liquids and PET fabrics, over which the bulk starts to form, plotted according to Eq. (3). Black, red, and blue points correspond to fabrics I, II, and III, respectively.

by a porous sheet without leaking a bulk flow. Then, we are able to determine the value experimentally by varying the flow rate supplied from a capillary, Q_i, with the pump. When Q_i exceeds Q_w, the liquid cannot be fully absorbed into the fabric and thus bulk drainage as shown in Fig. 3(c) occurs. For $Q_i < Q_w$, the wetting front propagates radially without bulk formation but at a lower rate than given in Eq. (1).

To quantify how the wicking behavior changes with Q_i, we first measure the rate of the wet area expansion, $\dot{A}_e$ through image analysis. We then compare the flow rate calculated based on the wet area expansion, $Q_e = \phi c \dot{A}_e$, with Q_i as shown in Fig. 4(a). For low Q_i, Q_e and Q_i are almost equal, locating the experimental points close to the straight line corresponding to $Q_e = Q_i$. At a very high liquid influx Q_i, Q_e fails to follow Q_i, moving the data points to the right of the straight line. In this case, Q_i exceeds the maximum wicking rate Q_w that the fabric can accommodate, thus the excess amount forms a bulk on top of the fabric surface, which eventually drains due to gravity. The highest value of Q_i's that are equal to Q_e corresponds to the threshold flow rate, Q_w, above which the bulk drainage occurs. Figure 4(b) plots the experimentally obtained values of Q_w for different liquids and porous materials, to show that it is indeed proportional to $c\sigma (1 - \phi) /(r_f \mu \phi)$ as predicted by Eq. (3).

We note that our theoretical development leads to a novel way to find κ through Eq. (3). The slopes of the straight lines in Fig. 4(b) give κ. Here, r_f and ϕ are measured with the optical microscope image and porosimeter (Autopore IV9500, Micromeritics), respectively. Compared with other methods to estimate in-plane permeability, especially the classical radial methods,[21–23] the current method does not require a pressure gauge, flow meter, nor setup to tightly fasten fabrics to prevent bulk leakage. κ can be estimated simply by measuring the critical flux at which flooding occurs.

IV. FLOODING PROFILE

For $Q_i > Q_w$, a bulk, or a rivulet with a finite thickness, runs downward while the wicking still takes place in the lateral direction, as shown in Fig. 3(c). We experimentally measure and explain the elongation rate of the rivulet and edge profile of the wet area when the flooding occurs. Since the excess flow rate $\Delta Q = Q_i - Q_w$, which cannot be absorbed into the fabric, grows the rivulet, the length of the rivulet is given by $l = \Delta Q t/(hw)$, where h and w are the average film thickness and width, respectively. Measuring a rivulet area and using volume conservation allows us to find h and w to be almost constant along the rivulet in the range of 0.8-1.2 mm and 4-6 mm, respectively, depending on the experimental condition. This finding is consistent with the following considerations. Let alone the fact that ΔQ is constant because both Q_i and Q_w are constant, the flow speed of rivulet is constant for the balance between gravitational and viscous forces, which is supported by the experiments. Furthermore, the wetting state is invariant while the rivulet runs due to continual contact with the pre-wetted surface.
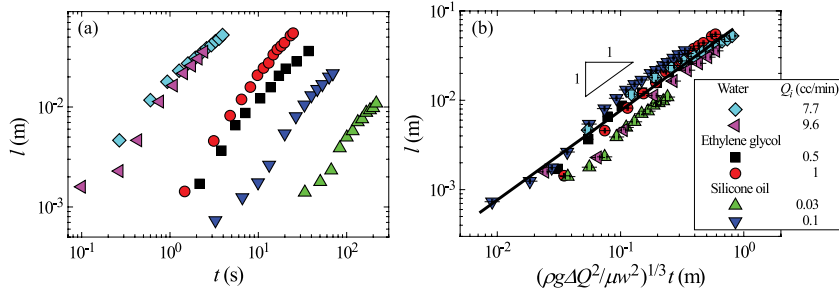
FIG. 5. Experimental results of flooding on fabric I. (a) Rivulet length versus time. (b) Rivulet length plotted according to the scaling law (4). The black line is the best fitting line with a slope of unity. Its intersection with the y-axis gives the value of C, 0.077.

Modeling the rivulet thickness with the thin film approximation due to $h \ll l$ except for the very initial stage, we balance viscous forces with gravitational forces to write $\mu U / h^2 \sim \rho g$ following Nusselt.[24] Here, U is the characteristic downward flow velocity, given by $U = \Delta Q/(hw)$, which leads to a scaling relation for h as $h \sim [\mu \Delta Q/(\rho g w)]^{1/3}$. Then, the elongation of the rivulet length can be scaled as

$$l \sim \left(\frac{\rho g \Delta Q^2}{\mu w^2} \right)^{1/3} t. \tag{4}$$

Figure 5(a) shows that the raw data of the rivulet length grow linearly with time for various liquids and flow rates. The data tend to cluster onto a straight line when plotted in log-log scale according to the scaling law (4) as shown in Fig. 5(b). Writing $l \approx C[\rho g \Delta Q^2/(\mu w^2)]^{1/3} t$, we empirically get $C = 0.077$, which in turn gives $h \approx 13[\mu \Delta Q/(\rho g w)]^{1/3}$. The scatter in Fig. 5(b) is supposed to be due to lateral curvature of the rivulet of finite width and variations of film thickness affected by the advancing front, which were not considered in Nusselt's model.

We now analyze the shape of a wet area formed by gravitational drainage on porous walls. Except for the very early stages when $\dot{l} < \dot{R}_w$ or $t < \kappa \sigma (w^4/g^2 \Delta Q^4 \mu \rho^2)^{1/3}/(r\phi)$, the elongation of the rivulet is faster than the wicking. Then, a vertically elongated blot around the rivulet grows in both vertical and horizontal directions in time as shown in Fig. 3(c). Based on the foregoing analysis of the wicking rate and rivulet growth, the following geometric considerations allow us to predict the blot shape. Consider three points P, Q, and R that the tip of rivulet passes at time $t = 0$, t_1, and t_2, respectively, as shown in Fig. 6(a). The distance between Q and R is given by $y_1 = \eta(t_2 - t_1)$, where $\eta = C(\rho g \Delta Q^2/\mu w^2)^{1/3}$ via (4). While the tip of rivulet travels from Q to R for $t_2 - t_1$, the furthest horizontal reach of the wicking front starting from Q is $x_1 = \zeta(t_2 - t_1)^{1/2} + 0.5w$, where $\zeta = 2\sqrt{\kappa(1-\phi)\sigma/(r_f \phi^2 \mu)}$ via Eq. (2). It naturally follows that x_1 and y_1 are related as $y_1 = (\eta/\zeta^2)(x_1 - 0.5w)^2$. Placing the origin of the reference frame at R to generalize this relationship, the equation of the wet area, which is symmetric about the y-axis, is thus given by

$$y = C \frac{r_f \phi^2}{4\kappa\sigma(1-\phi)} \left(\frac{\rho g \mu^2 \Delta Q^2}{w^2} \right)^{1/3} \left(x - \frac{w}{2} \right)^2 \quad \text{for } |x| > \frac{w}{2}. \tag{5}$$

The rivulet of the width w is expressed as $y = 0$ for $|x| < w/2$. Here, we have ignored the flow through the porous medium under gravity for negligible gravitational effects compared to the capillary forces ($r \ll l_c$). Thus, the wicking front expansion occurs owing to the liquid supply from the reservoir of liquid in the centerline.[25]

Two salient features stand out in Eq. (5): the wet front keeps its parabolic profile regardless of time, and the area gets narrower with the increase of ΔQ and μ but with the decrease of κ and σ. Figure 6(b) shows that the experimentally measured shapes of a growing wet front at different times match well with our theory. The experimentally measured effects of the flow rate on the width of the wet area are displayed in Fig. 6(c), showing good agreement with our theory as well.
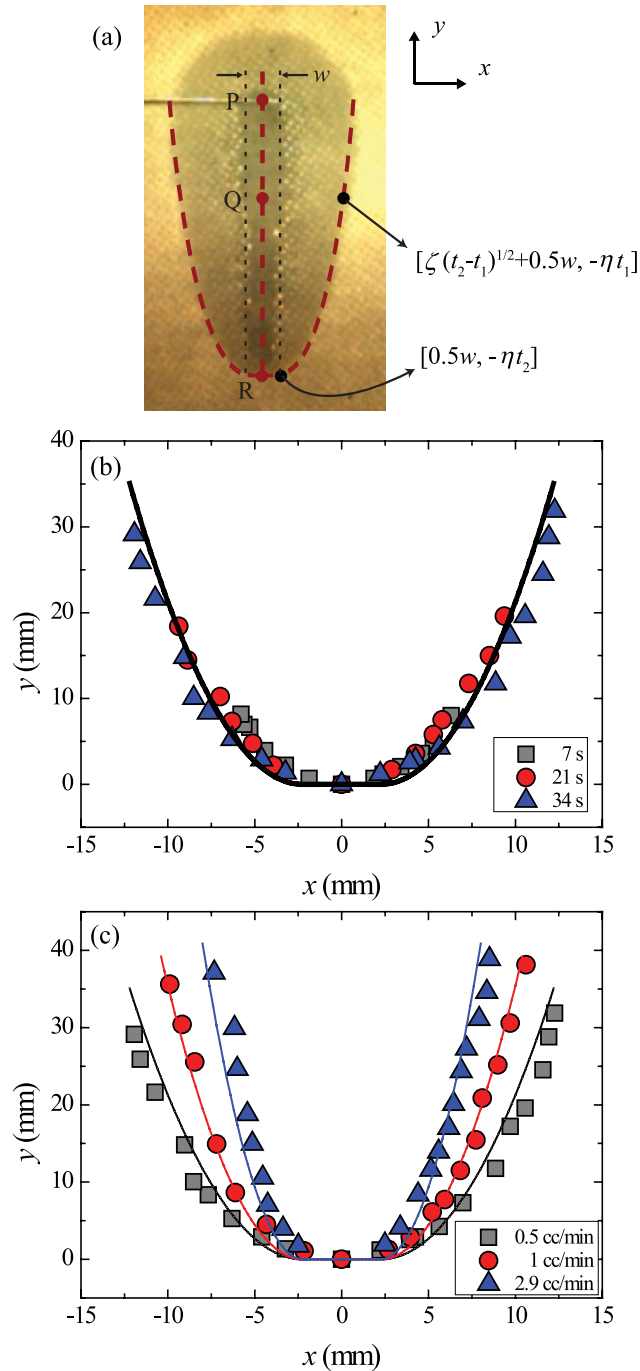
FIG. 6. (a) The coordinate system for the analysis of the shape of wet area in case of flooding. (b) The measured wet front profile follows Eq. (5) for different t. The experiments were carried out using fabric I and ethylene glycol with $Q_i = 0.5$ cc/min. (c) The wet area becomes narrower as Q_i increases, but its profile still follows Eq. (5). In (b) and (c), the solid lines correspond to the theoretical predictions.

V. CONCLUSIONS

We have studied the dynamics of liquid fed from a point source onto a vertically situated, hydrophilic fabric sheet. While a circular wicking front develops for low flow rates, a bulk emerges as the feeding rate exceeds a critical value, Q_w. Using the Darcy law, we have obtained Q_w as

a function of the liquid and fabric properties. Since Q_w can be precisely determined by using a syringe pump that controls the liquid feeding rate, we can obtain an estimate of the in-plane permeability of a porous sheet in a simpler manner compared to conventional methods. The shape of a wet area formed when the flow rate exceeds Q_w has been analyzed based on the dynamic model of wicking. It is found that while the rivulet length grows linearly with time, the parabolic wetting front around the rivulet does not change its nose shape with time. The functional dependence of the wet area profile on such parameters as the flow rate, viscosity, surface tension, and the fabric properties has been given. Besides serving as a model problem to understand the running watercolor on a vertical paper, this study can be used to design highly effective liquid-absorbing porous sheets and to predict liquid flow profiles on them in such applications as HVAC equipments and fuel cell membranes.

ACKNOWLEDGMENTS

[1] K. M. Pillai and S. G. Advani, "Wicking across a fiber-bank," J. Colloid Interface Sci. **183**, 100-110 (1996).

[2] A. W. Martinez, S. T. Phillips, and G. M. Whitesides, "Three-dimensional microfluidic devices fabricated in layered paper and tape," Proc. Natl. Acad. Sci. U. S. A. **105**, 19606-19611 (2008).

[3] M. Landeryou, I. Eames, and A. Cottenden, "Infiltration into inclined fibrous sheets," J. Fluid Mech. **529**, 173-193 (2005).

[4] X. Ma, G. Ding, Y. Zhang, and K. Wang, "Airside characteristics of heat, mass transfer and pressure drop for heat exchangers of tube-in hydrophilic coating wavy fin under dehumidifying conditions," Int. J. Heat Mass Transfer **52**, 4358-4370 (2009).

[5] A. Lee, M. W. Moon, H. Lim, W. D. Kim, and H.-Y. Kim, "Water harvest via dewing," Langmuir **28**, 10183-10191 (2012).

[6] A. Tamayol and M. Bahrami, "Water permeation through gas diffusion layers of proton exchange membrane fuel cells," J. Power Sources **196**, 6356-6361 (2011).

[7] W. C. Sherbrooke, *Introduction to Horned Lizards of North America* (University of California Press, Berkeley, CA, 2003).

[8] C. Gans, R. Merlin, and W. F. C. Blumer, "The water-collecting mechanism of *Moloch horridus* re-examined," Amphibia-Reptilia **3**, 57 (1982).

[9] S. Schiaffino and A. A. Sonin, "Molten drop deposition and solidification at low Weber numbers," Phys. Fluids **9**, 3172-3187 (1997).

[10] N. Mao and S. J. Russell, "Capillary pressure and liquid wicking in three-dimensional nonwoven materials," J. Appl. Phys. **104**, 034911 (2008).

[11] G. W. Jackson and D. F. James, "The permeability of fibrous porous media," Can. J. Chem. Eng. **64**, 364 (1986).

[12] P. Xu and B. M. Yu, "Developing a new form of permeability and Kozeny-Carman constant for homogeneous porous media by means of fractal geometry," Adv. Water Resour. **31**, 74-81 (2008).

[13] N. Mao, "Permeability in engineered non-woven fabrics having patterned structure," Text. Res. J. **79**, 1348-1357 (2009).

[14] A. Nabovati, E. W. Llewellin, and A. C. M. Sousa, "A general model for the permeability of fibrous porous media based on fluid flow simulations using the lattice Boltzmann method," Composites Part A **40**, 860-869 (2009).

[15] C. H. Shih and L. J. Lee, "Effect of fiber architecture on permeability in liquid composite molding," Polym. Compos. **19**, 626-639 (1998).

[16] G. Løvoll, Y. Méheust, K. J. Måløy, E. Aker, and J. Schmittbuhl, "Competition of gravity, capillary and viscous forces during drainage in a two-dimensional porous medium, a pore scale study," Energy **30**, 861-872 (2005).

[17] H. E. Huppert and A. W. Woods, "Gravity-driven flows in porous layers," J. Fluid Mech. **292**, 55-69 (1995).

[18] D. Vella and H. E. Huppert, "Gravity currents in a porous medium at an inclined plane," J. Fluid Mech. **555**, 353-362 (2006).

[19] E. W. Washburn, "The dynamics of capillary flow," Phys. Rev. **17**, 273 (1921).

[20] J. Kim, M.-W. Moon, K.-R. Lee, L. Mahadevan, and H.-Y. Kim, "Hydrodynamics of writing with ink," Phys. Rev. Lett. **107**, 264501 (2011).

[21] H. Tan and K. M. Pillai, "A method to estimate the accuracy of radial flow-based permeability measuring devices," J. Compos. Mater. **43**, 2307-2332 (2009).

[22] G. W. Scherer, J. J. Valenza, and G. Simmons, "New methods to measure liquid permeability in porous materials," Cem. Concr. Res. **37**, 386-397 (2007).

[23] J. R. Weitzenbock, R. A. Shenoi, and P. A. Wilson, "Radial flow permeability measurement. Part B: Application," Composites Part A **30**, 797-813 (1999).

[24] W. Nusselt, "The condensation of steam on cooled surfaces," Z. Ver. Dtsch. Ing. **60**, 541-546 (1916).

[25] S. J. Kim, M.-W. Moon, K.-R. Lee, D.-Y. Lee, Y. S. Chang, and H.-Y. Kim, "Liquid spreading on superhydrophilic micropillar arrays," J. Fluid Mech. **680**, 477-487 (2011).